

Hydrogen-Bond-Mediated Phase Behavior of Complexes of Small Molecule Additives with Poly(ethylene oxide-*b*-propylene oxide-*b*-ethylene oxide) Triblock Copolymer Surfactants

Vikram K. Daga[†] and James J. Watkins^{*,‡}

[†]Department of Chemical Engineering and [‡]Department of Polymer Science and Engineering, University of Massachusetts, Amherst, Massachusetts 01003, United States

Received July 27, 2010; Revised Manuscript Received October 15, 2010

ABSTRACT: The addition of multifunctional additives comprised of single- or double-ring aromatic cores decorated at their periphery with multiple hydrogen-bond-donating groups such as carboxylic acid and phenol is shown to induce microphase segregation of otherwise disordered Pluronic BCP (poly(ethylene oxide–propylene oxide–ethylene oxide)) surfactant melts, resulting in the formation of well-ordered supramolecular assemblies with domain spacings ranging between 12.5 and 14.5 nm at additive loadings up to 40%. As the concentration of additives is increased, the general tendency is that the disordered system evolves into an ordered morphology and then undergoes an order–order transition before transitioning into a disordered phase, in one case. The scaling of interplanar spacing reveals that the additives are selectively incorporated in the poly(ethylene oxide) phase. Differential scanning calorimetry indicated that progressive increases in the loading of additives causes a decrease in the melting temperature and melting enthalpy of poly(ethylene oxide) crystallites. This behavior is consistent with good dispersion and strong interaction of the additives with the poly(ethylene oxide) phase. The principles invoked in this additive driven assembly process can be generally applied to the design of ordered functional BCP–nanoparticle hybrid materials while the specific materials described here could be of interest as etch masks.

Introduction

Self-assembly of block copolymers (BCPs) can yield nanostructured polymeric materials containing periodically arranged nanoscale domains.^{1–3} Many applications of BCPs could emerge due to differences in the chemical and/or physical properties of the various phases present in a self-assembled BCP material or BCP-templated composite. For example, BCPs have attracted attention as low line edge roughness resists for nanoscale electronics⁴ and as templates for the fabrication of nanoscale microelectronic structures including high density data storage media.^{5–7} BCPs have also been used as templates to carry out phase selective reactions for the fabrication of inorganic mesostructured materials,^{8–10} and phase selective treatments of BCPs have been performed to remove the minority phase, or a component of it, to form nanoporous polymeric materials.^{11–13} BCPs have been used to direct the organization of hybrid materials, including polymer/nanoparticle composites.^{14,15} These materials have generated significant interest due to their potential in emerging areas such as photovoltaics^{16–18} and photonics.^{19–21} A recent review summarizes the advances in employing BCP nanostructures in electronics.²² Incorporation of additives such as homopolymers, nanoparticles, and small molecules selectively into BCP domains is advantageous as it not only imparts a desired functionality but also can be used to gradually alter morphology and domain spacing without a need for synthesis of new BCPs for each of the states obtained.

Microphase separation of BCPs is thermodynamically governed by the product χN , where χ is the Flory–Huggins interaction parameter between segments of the dissimilar blocks and N is the total number of repeat units. When the segregation strength is

high, BCPs containing two chemically dissimilar blocks (i.e., A–B, A–B–A, A–B–A–B, and so on) form spherical, cylindrical, and lamellar morphologies as determined mainly by the relative volume fractions of A and B phases.^{1,2} For a particular volume fraction, the critical segregation strength required for microphase separation increases as the number of blocks increase. For example, for symmetric BCPs, i.e., for BCPs with equal volume fraction of A and B blocks, phase segregation of A and B blocks of A–B diblock copolymer occurs when segregation strength exceeds 10.5,² while A–B–A type triblock copolymer requires a segregation strength of greater than 18 for microphase separation.^{23,24} When these critical values are not met due to a small χ and/or N , the BCP remains disordered. This is the case for the neat BCP employed in the present work. Additionally, as BCPs become increasingly asymmetric with respect to the relative volume fraction of the blocks, the critical segregation strength for microphase separation increases rapidly as evidenced by a steep shift in the phase boundary. Therefore, regardless of how high the segregation strength is, as the volume fraction of A block is increased sufficiently at the expense of B block, a point will be reached when the BCP can no longer order. One of the BCP systems shown in this work undergoes this kind of order-to-disorder transition (ODT) at higher additive loadings (see behavior of blends of CTMA and F108 in Results section).

Many applications would benefit from small domain sizes and, in the case of hybrid materials, high additive loadings. One challenge for achieving small domain sizes is that decreases in molar mass required to decrease the interdomain spacing also weaken the segregation strength. It is often more desirable to increase the interaction parameter to maintain strong segregation. For hybrid materials, it is further desirable to maintain strong phase segregation and order upon the selective addition of additives to one domain of microphase-segregated BCP

*Corresponding author. E-mail: watkins@polysci.umass.edu.

templates. Unfortunately, the amount of additives, especially nanoparticles, that can be incorporated into BCPs can be limited as high loadings can disrupt the ordered BCP structure due to entropic penalties associated with polymer chain stretching required to accommodate the additives.²⁵ In addition, lack of sufficient interaction between the additive and the polymer chain can cause the additives to aggregate, which can lead to the loss of BCP order due to excessive chain stretching which would be required to accommodate large aggregates.²⁶

A rich phase behavior has been observed when selectively associating small molecule additives are blended into microphase-segregated BCPs. As described in a recent literature,^{27,28} order-to-order transitions (OOT) and disorder-to-order transitions occur upon addition of small molecules like 3-*n*-pentadecylphenol to polystyrene–polyvinylpyridine (PS–PVP) and polyisoprene–polyvinylpyridine BCPs to obtain well-ordered morphologies in bulk as well as in thin films.^{29,30} Such additive molecules exhibit phenol groups at one end which enable their supramolecular association with the PVP block through hydrogen-bonding interactions.²⁷ These additive molecules also exhibit long noninteracting alkyl chains that provide access to a complex and varied phase behavior. For example, within a temperature window, microphase separation of alkyl chains from the other phases causes formation of separate domains within the block copolymer domains.^{31,32} In contrast, here we focus on small molecule additives in which the noninteracting cores are functionalized around their periphery with groups that can form hydrogen bonds to a particular block of the copolymer. This design strategy should enable incorporation of the additive within one domain as the aromatic core is “shielded” from unfavorable interactions with the host domain. As shown here, such a strategy can preserve the native morphologies of block copolymers while allowing high additive loadings. The ability to functionalize a phase uniformly without formation of hierarchical structures is important to many applications such as block copolymer electrolytes,³³ in which well-defined ion conduction pathways are desired, or block copolymer lithography,³⁴ which relies on the difference in etch contrast of the different BCP phases. Non-polymeric additives that do not lead to formation of substructures within BCP domains have also been demonstrated to affect BCP morphology. One example of such an additive is 2-(4'-hydroxybenzenazo)benzoic acid, which has been used with PS–PVP to control domain orientation and as a means to generate porous structures by subsequent removal of the additive.^{13,35–38} In contrast to using hydrogen-bonding interactions, ionic complexation of lithium^{39–41} and gold⁵ salts with PEO has also been demonstrated to modify the phase behavior of PEO containing BCPs.

Likewise, several studies have focused on incorporation of homopolymers into BCPs in which the observed phase behavior of the blend was found to vary gradually depending upon the composition and chain length of homopolymers. For example, Hashimoto and co-workers examined polystyrene–polyisoprene BCPs with polystyrene and/or polyisoprene homopolymers as additives.^{42,43} Because the interaction between the homopolymer additive and the incorporating block is athermal in this case, the phase behavior of such blends is governed primarily by entropic factors. Thus, low molecular weight homopolymers mix homogeneously with the incorporating block because of favorable entropy of mixing but larger homopolymers localize toward the center of the incorporating block to minimize the loss in entropy caused by stretching of the BCP and homopolymer chains. Because of homogeneous mixing, as the loading of small homopolymer additives is increased, a smaller change in domain spacing occurs but the system undergoes OOT, while due to localized mixing, sufficiently large homopolymers cause a larger change in domain spacing but do not cause OOT.⁴² The lack of

strong interaction between the homopolymer and the incorporating block also sets a low limit on the size of homopolymers above which they macrophase separate from the BCP. For example, macrophase separation of poly(methyl methacrylate) homopolymer occurs from polystyrene–poly(methyl methacrylate) block copolymer when the ratio of chain lengths of the homopolymer to the molecular weight of BCP exceeds about 1.0.⁴⁴

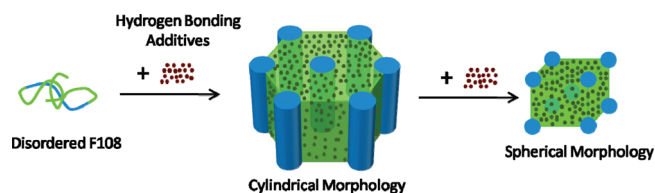
In contrast, strong interactions between the additive homopolymer and incorporating block can facilitate incorporation of high loadings of even large homopolymers as the favorable enthalpic interactions can offset the entropic penalty associated with stretching of large homopolymers.⁴⁴ Recently, we reported that the addition of homopolymers that selectively associate through hydrogen bonding with the PEO blocks of disordered Pluronic triblock copolymer surfactants (PEO–PPO–PEO) induces microphase segregation and strong order.^{9,45,46} Phase segregation in the blends is driven by the strong attractive interactions of the homopolymers with the PEO blocks, and the system assembles to maximize the energetically favorable interactions between PEO and homopolymer, which results in exclusion of PPO from the PEO–homopolymer phase and ultimately leads to the formation of well-ordered BCP morphologies. For the case of Pluronic BCP surfactant, P105 (EO₃₇–PO₅₆–EO₃₇, 6.5 kg/mol) blending of 20% to 50% poly(acrylic acid) (PAA) of molecular weights ranging between 2 and 88 kg/mol caused ordering and OOT in all cases.⁴⁵ Thus, in contrast to the above-mentioned chain ratio limit of about 1.0 for achieving incorporation of a weakly interacting homopolymer, homopolymer chains significantly larger than the BCP could be incorporated in this case. However, when 1-propanoic acid, a small molecule analogous to a single repeat unit of PAA, was blended with P105, the system remained disordered. The use of hydrogen bonding as a means to mediate interactions of polymers and additives is advantageous because the strength of interaction and hence the structure and properties of such blends can be controlled by varying the nature of the functional groups placed on the additive molecules as well as by varying the temperature.

In this work we report an important extension of the phenomenon ordering of Pluronic surfactants with associating homopolymers. We establish that non-polymeric, small molecule additives that contain multiple hydrogen-bonding sites such as phenol or carboxylic acid groups at their periphery can likewise induce order in Pluronic BCP F108 (EO₁₂₇–PO₄₈–EO₁₂₇), resulting in formation of well-ordered materials at additive loadings up to 40% (Scheme 1). In comparison to homopolymer additives, non-polymeric additives offer more structural, chemical, and functional flexibility in functionalization of BCPs. A vast array of small molecules bearing such hydrogen-bonding groups exist, and the ones employed here only represent a few possible structures. Since small molecules are monodisperse in their size and structure, they also allow a systematic study by providing a precise control on the size of additive molecules and the number and type of functional groups. We expect that the principles established here will be of general utility for the design and preparation of well-ordered composite materials.

Materials and Methods

Materials. Pluronic F108 (EO₁₂₇–PO₄₈–EO₁₂₇, 14.6 kg/mol) which contains about 80 wt % EO is a commercially available commodity surfactant and was donated by BASF. Using gel permeation chromatography, the PDI of F108 was found to be 1.18. Benzene-1,2,3,4,5,6-hexacarboxylic acid (BHCA, $M_w = 342$ g/mol) and benzene-1,2,3,4,5,6-hexol (HHB, $M_w = 174$ g/mol) were purchased from TCI America. 5,5'-Carbonylbis(trimellitic acid) (CTMA, $M_w = 446$ g/mol) was purchased from Sigma-Aldrich. *N,N*-Dimethylformamide (DMF) and water

Scheme 1. Schematic Representation of Additive Driven Assembly of Disordered F108 Induced by Blending with Hydrogen-Bond-Donating Small Molecule Additives^a



^aPEO in green forms the matrix containing the dispersed small molecule additive. PPO in blue forms the minority domain, either cylinders or spheres.

were purchased from Fisher Scientific. All the materials and solvents were used as received.

Sample Preparation. Appropriate amounts of F108 and additives were dissolved in DMF to form 10 wt % solids solutions on a hot plate set to 65 °C. For the case of blends of F108 and BHCA, a 1:1 ratio by weight water–DMF mixture was used as the solvent. The solutions were drop-casted on glass slides and kept inside a vacuum oven maintained at 75 °C for 36–48 h. Solvent mass losses were tracked to confirm that the resulting samples did not contain any residual solvent. In this work, compositions are reported as weight ratios of additive to F108. For example, a blend referred to as 30/70 contains 30% additive and 70% F108 by weight.

Small-Angle X-ray Scattering. The dried samples were placed in the center of 1 mm thick metal washers and sealed on both sides with Kapton film. The filled metal washers were maintained at 80 °C on a heating stage from Linkam equipped with TMS94 temperature controller. A 30 min equilibration time at 80 °C was employed before the measurements which were conducted for each sample for 1 h. Small-angle X-ray scattering (SAXS) was performed using an instrument from Molecular Metrology Inc. (presently sold as Rigaku S-Max3000) using 0.1542 nm (Cu K α radiation) and an incident beam of 0.4 mm diameter. The sample-to-detector distance was calibrated using silver behenate standard peak at 1.076 nm⁻¹. The setup employs a two-dimensional gas-filled wire detector for collection of scattered X-ray and allows measurements in wave vector (q) range of $0.06 < q < 1.6 \text{ nm}^{-1}$ in which $q = (4\pi/\lambda) \sin \theta$, where 2θ is the scattering angle. The raw scattering data were circularly averaged and plotted as intensity vs q where intensity was used in arbitrary units. For data presentation, the profiles are shifted vertically by multiplying intensity values with constant factors to avoid overlap of the profiles.

Differential Scanning Calorimetry. The blends prepared for SAXS were used for DSC to obtain complementary data. Sample masses of 10–15 mg were filled into aluminum pans and hermetically sealed. DSC thermograms were measured using a TA Instruments Q100 DSC equipped with an RCS cooling system and nitrogen gas purge with a flow rate of 50 mL/min. All measurements were conducted in the temperature range of –90 to 80 °C at a constant heating and cooling rate of 10 °C/min under a nitrogen atmosphere. Temperature calibration was carried out using indium as a standard ($T_m = 156.6 \text{ °C}$) and the indium heat of fusion (28.6 J/g) was used to calibrate the heat flow. The reported DSC thermograms were measured during second heating cycle. With the exception of neat F108 the thermograms of the samples are shifted vertically for data presentation. The constants added for this vertical shifting are reported. Universal analysis software was used to calculate the melting enthalpy and the melting temperature associated with the PEO melting endotherm. The calculated melting enthalpies were normalized with respect to the weight of PEO in the blend.

Results and Discussion

The small molecule additives blended with F108 are shown in Figure 1. This set of molecules allows study of the phase behavior

as a function of the identities of the hydrogen-bond-donating groups and of the size of the noninteracting cores at progressive additive loadings. BHCA and HHB allow comparison of the behavior of carboxylic acid groups vs phenol groups in ordering F108 as they both have the same core and the same number of hydrogen-bonding groups. Comparison between BHCA and CTMA illustrates the differences occurring due to varying the core size while maintaining the same number of carboxylic acid groups on additive molecules.

In order to test the capability of the additives to induce ordering of F108, the phase behavior of their blends was assessed using SAXS. Figure 2 shows the SAXS profiles for neat F108 and its blends with BHCA at varying compositions ranging up to 40% in which the disordered state and cylindrical and spherical morphologies are denoted by letters D, C, and S in parentheses beside the respective profiles. The SAXS profile of F108 shows a broad peak which is due to the correlation hole effect observed for disordered BCPs.^{2,47} This is expected as F108 is expected to be disordered at the measurement temperature of 80 °C.⁴⁸ As BHCA is blended, the peak gradually sharpens, indicating an apparent increase in the segregation strength, χN , between the PEO and PPO blocks. At 10% loading of BHCA the blend is ordered as indicated by a sharp primary peak together with appearance of a higher order peak. Multiple higher order peaks at 30% BHCA loading indicate formation of well-ordered cylindrical morphology. Thus, loadings of BHCA from 10% to 30% resulted in formation of cylindrical morphology. Since F108 is PEO-rich, PEO + BHCA form the matrix whereas PPO forms the cylindrical domains. As more BHCA was incorporated, the morphology of the blend transitioned into well-ordered spherical morphology at 40% loading. Thus, on a BCP phase diagram, the state of blends of F108 and BHCA traverses from disordered to cylindrical morphology to spherical morphology regions as the loading of BHCA increases progressively.

While neat F108 is disordered at 80 °C, the favorable enthalpic interactions created by maximizing the number of contacts between the additive and the PEO chains drive the disorder-to-order transition for blends of F108 with BHCA, resulting in an increase in the ODT temperature. As shown in the Supporting Information, the effect of weakening the hydrogen bond strength by increasing the temperature was explored for blends containing 10% and 20% BHCA between 60 and 120 °C. The 10% BHCA blend was found to be ordered at 100 °C but disordered at 120 °C, indicating that the ODT temperature of this blend falls between 100 and 120 °C. The 20% BHCA blend remained ordered up to 120 °C, indicating that the ODT should be higher than 120 °C. For the case of 20% BHCA blend since there are more additive molecules present, a larger number of hydrogen bond associations are possible for PEO chains which are sufficient to maintain order up to 120 °C. It is expected that blends containing 20% or more BHCA would disorder at an even higher temperature, but we did not identify the ODT temperatures in these cases as experiments at greater than 120 °C are complicated by reaction of the carboxylic acid groups to produce anhydrides.⁴⁹ In comparison, as expected, the neat F108 is disordered between 60 and 120 °C, as shown in the Supporting Information.

A closer look at the scattering profiles with increasing BHCA loading reveals some important features of the phase behavior of the composite. The continuous progression in the location of the primary peak (d -spacing of the composite) and the appearance of an OOT from cylindrical to spherical morphology are consistent with molecular level incorporation of BHCA in F108. The analysis of the data also suggests that BHCA exhibits limited compatibility with the PEO domains at high additive loadings. The SAXS data suggest that the maximum BHCA loading is about 40% as the SAXS profile for 50% loading of BHCA matched in peak positions and morphology to that obtained for

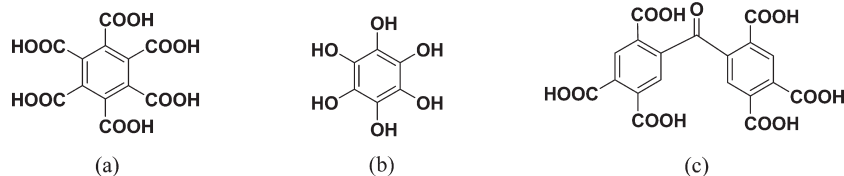


Figure 1. Hydrogen-bond-donating additives incorporated into the PEO phase of F108: (a) benzene-1,2,3,4,5,6-hexacarboxylic acid (BHCA), (b) benzene-1,2,3,4,5,6-hexol (HHB), (c) 5,5'-carbonylbis(trimellitic acid) (CTMA).

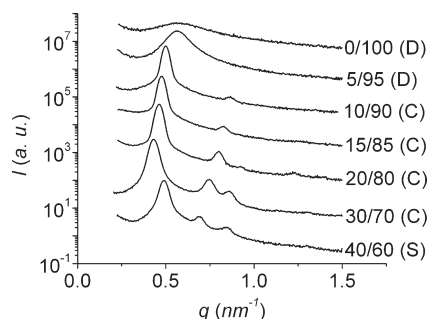


Figure 2. SAXS profiles of blends of F108 and benzene-1,2,3,4,5,6-hexacarboxylic acid (BHCA) as a function of composition at 80 °C. The disordered state and cylindrical and spherical morphologies of the blends are denoted by D, C, and S, respectively.

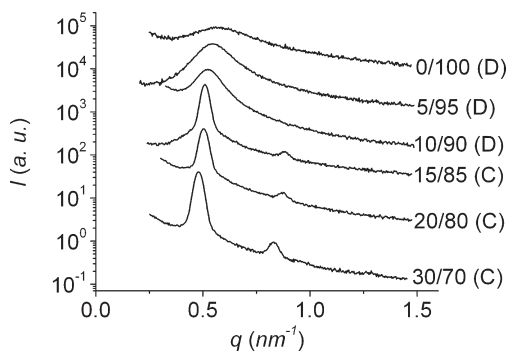


Figure 3. SAXS profiles of neat F108 and its blend with 30% benzene-1,2,3,4,5,6-hexol (HHB) at 80 °C. The disordered state and cylindrical and spherical morphologies of the blends are denoted by D, C, and S, respectively.

40% loading, suggesting that addition of BHCA above this point leads to macrophase segregation. This system was therefore studied up to 40% loading of BHCA. Furthermore, in addition to indicating molecular level incorporation of BHCA, occurrence of OOT from cylindrical to spherical morphology between 30% and 40% loading of BHCA indicates qualitatively that the incorporation of BHCA must be selective toward PEO, thereby causing a reduction in the relative volume fraction of the PPO phase leading to formation of spherical morphology. Scaling of interplanar spacing with composition as discussed later further suggests that this indeed is the case.

We next explore the effect of the nature of hydrogen-bond-donating group (i.e., carboxylic acid vs phenol groups) of the additive molecules on the ordering of F108 by comparing the behavior of the BHCA and HHB additives. Since the interaction of additive molecules with PEO chains drives the ordering of F108, a change in the functional group must affect the strength of interaction, which should affect the incorporation of additives and the consequent phase behavior. Figure 3 shows the scattering profiles of blends of F108 with HHB loaded up to 30%. Qualitatively, the phase behavior of HHB blends is similar to that

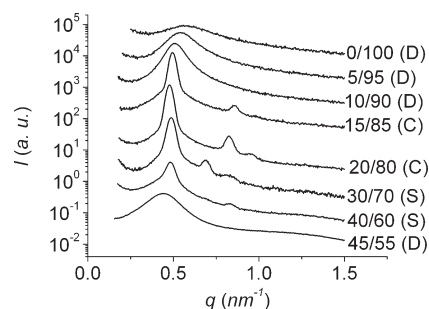


Figure 4. SAXS profiles of neat F108 and its blends with 5,5'-carbonylbis(trimellitic acid) (CTMA) as a function of composition at 80 °C. The disordered state and cylindrical and spherical morphologies of the blends are denoted by D, C, and S, respectively.

observed with BHCA. The broad correlation hole peak of neat F108 sharpens into a primary peak and higher order peaks appear as HHB composition increases, indicating disorder-to-order transition due to enhanced segregation strength between PEO and PPO chains. However, the change in segregation strength upon addition of HHB to F108 is found to be less than that with BHCA. This can be seen by comparing the SAXS profiles at 10% loading in both cases. While 10% BHCA caused formation of well-ordered morphology, 10% HHB blend is not ordered even though the number of carboxylic acid groups contributed by BHCA per equivalent volume fraction of additive is less because of its higher molecular weight than HHB. Thus, carboxylic acid groups are found to be more efficient at causing ordering of F108 than phenol groups which seems to indicate that, as compared to phenol groups, carboxylic acid groups interact more strongly with the ether oxygen of PEO. Upon addition of 15–30% loading of HHB, an ordered cylindrical morphology appears similar to that seen for BHCA at the same loadings. The scattering profiles of blends with loadings higher than 30% did not show variation in position of primary peak or OOT, and therefore the saturation level of HHB in F108 must be close to 30%. Thus, by comparison, the carboxylic acid functionality was slightly more effective for achieving high additive loading as compared to phenol functionality.

Next, the effect of increasing core size of additive molecule while maintaining the same number of hydrogen-bonding interaction sites on each molecule was explored by comparing the behavior of BHCA and CTMA for which the core size is about double that of BHCA. The SAXS profiles obtained for blends of F108 with CTMA are shown in Figure 4. As the size of the core is increased while maintaining the same number of carboxylic acid groups, the number of available carboxylic acid groups added is decreased at a particular additive loading. This impacts segregation strength, and at a 10% loading, while the BHCA blend is ordered, the CTMA blend is not yet ordered. By comparison to BHCA, the range of composition within which CTMA blends form cylindrical morphology is smaller. While the 30% BHCA blend shows cylindrical morphology, the 30% CTMA blend showed spherical morphology. This implies that simply by varying the molecular structure of the additives the resulting

blend morphology may be varied at the same additive loading, i.e., at the same relative volume fraction of the two phases formed. A transition from cylindrical to spherical morphology should occur at a point when the entropic penalty of stretching the PEO and PPO chains away from the interface exceeds the entropic penalty in causing additional interfacial curvature in transitioning from cylindrical to spherical morphology.⁴³ The OOT occurs at a lower composition of CTMA than BHCA, which may imply a larger capacity of CTMA to affect chain density at the interface and thus the chain stretching. This in turn may imply that CTMA is present closer to the PEO–PPO interface than BHCA. CTMA blends showed systematically varying scattering profiles up to 45% loading without any signs of macrophase separation. In contrast, as described earlier, the saturation level for BHCA and HHB was found to be 40% and 30%, respectively. At 45% loading a disordered blend resulted, implying that the relative volume fraction changed sufficiently to bring the system into disordered region.

Comparison of the full width at half-maximum (FWHM) of the primary peaks of the SAXS profiles provides a comparison of the degree of order in BCP systems.^{38,46} Smaller FWHM corresponds to a higher degree of segregation and overall order. The primary peaks for all blends were fitted to a Gaussian curve, and the values of FWHM obtained were plotted against blend compositions as shown in Figure 5.⁵⁰ For all additives, the FWHM value decreases from that of neat F108, indicating an increase in segregation strength upon addition of additives. At lower loadings, BHCA blends show the largest drop in FWHM which indicates that BHCA has the highest tendency to cause phase segregation of F108. The FWHM values of CTMA and HHB blends are larger than BHCA with that of CTMA being slightly less than that of HHB. The FWHM values decreases rapidly initially with loading of additives, indicating a sudden jump as disorder-to-order transition occurs and then follows a slowly increasing trend with further increase in the loading of additives. After the initial dramatic reduction in FWHM, the FWHM for

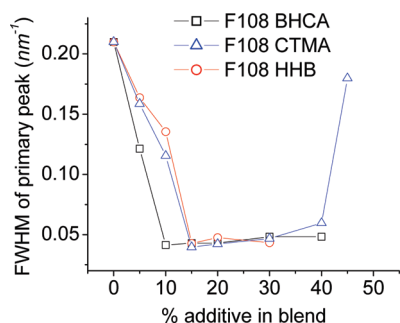
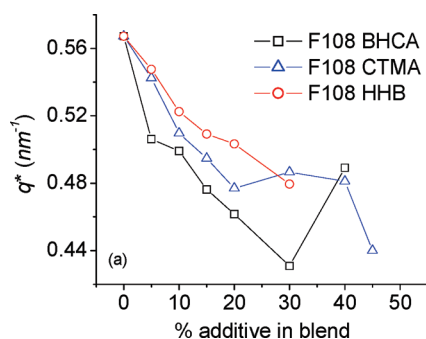


Figure 5. Full width at half-maximum (FWHM) of the primary scattering peaks for blends of F108 with BHCA, HHB, and CTMA.



blends with different additives are comparable in the intermediate composition range (probably due to detector resolution limit) and preclude any comparison. Even so, as seen next, the primary peak positions provide a comparison between segregation strengths induced by various additives. The FWHM of CTMA covered the entire range of behavior, i.e., initial rapid decrease, followed by a gradual increase in the ordered region and then a rapid increase at high loadings implying order-to-disorder transition.

Figure 6a compares the variation of primary peak position, q^* , for all blends. The value of q^* is the smallest for BHCA and largest for HHB within a particular morphology with CTMA falling in between. A sudden increase in the q^* value at 40% for BHCA and at 30% for CTMA is due to OOT from cylindrical to spherical morphology while HHB blends remained cylindrical in the composition range explored. The interplanar spacing between 100 planes of blends forming cylindrical morphology was estimated as $2\pi/q^*$ and plotted against the weight fraction of F108 on a log–log scale in Figure 6b. The value of scaling exponent β in the relation $d \sim \phi_p^{-\beta}$ of interplanar spacing (d) vs volume fraction of BCP (ϕ_p) can be useful in identifying the selectivity of the additives.⁵¹ A positive value of β indicates selectivity of additives toward one of the phases. In this work, assuming that the density of additives is the same as the density of F108, the interplanar spacing vs volume fraction for the blends formed with the three additives has been fitted as shown in Figure 6b according to the relation

$$d = A\phi_p^{-\beta}$$

where the prefactor A represents a hypothetical interplanar spacing of neat F108 had it been ordered. The value of A was set to 11.852 nm, and the d vs ϕ_p data were fitted to estimate the β exponents. This value of A was found to minimize the sum of squares of residuals for all the three fittings.⁵² The values of scaling exponent, β , for the case of BHCA, HHB, and CTMA were found to be 0.595, 0.264, and 0.455, respectively. Compared to values in the literature for other systems,⁵¹ such positive and high values indicate strong selectivity of the additives toward PEO phase as the systems order. Although these values are estimated assuming that the density of additive molecules are the same as that of F108, the scaling exponents could be estimated more precisely by using liquidlike densities as the density of additives. However, such values are not reported in part because BHCA and CTMA contain carboxylic acid groups which undergo dehydration below melting temperature. Since additive molecules interact favorably among themselves via hydrogen bonding, the liquidlike densities of additives are expected to be at least as small as F108 if not higher. If the densities of the additives were higher than that of F108, even higher β exponents would result. Therefore, the values estimated above represent the lower bounds

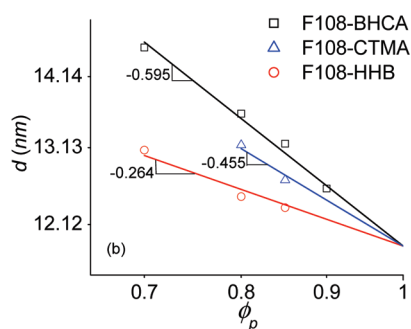


Figure 6. Comparison of behavior of BHCA, HHB, and CTMA additives: (a) variation of position of primary peak for blends; (b) scaling of interplanar spacing (d) with composition (ϕ_p) for blends that formed cylindrical morphologies.

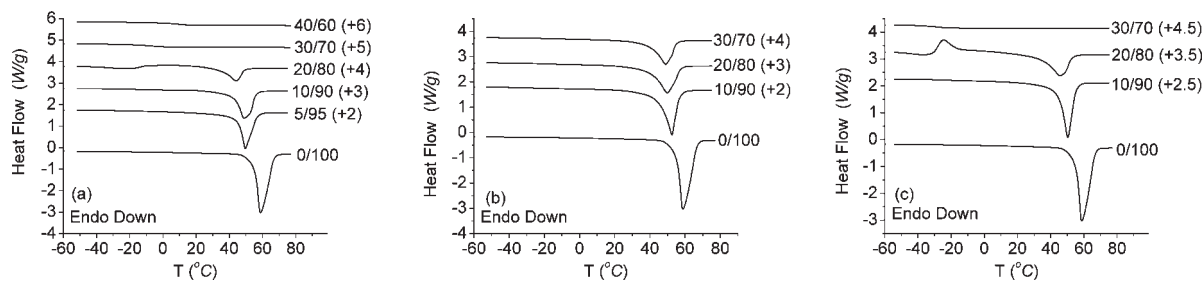


Figure 7. DSC thermograms of neat F108 and its blend with (a) BHCA, (b) HHB, and (c) CTMA. The constants added to the heat flow values to shift the blend thermograms vertically upward are shown in parentheses.

of the scaling exponents. Although all the three additives are strongly selective toward the PEO phase, their blends differ in the domain spacings formed at the same loadings. This is attributed to the differences in the capacity of the additives to enhance the segregation strength. As segregation strength increases, the domain interface becomes narrower and the polymer chains stretch farther away from the domain interface leading to larger domain spacing. Such a behavior is commonly observed in other BCP systems in which temperature-dependent variations in segregation strength shift the domain spacing.^{53–55} Similar behavior is observed for the 10% and 20% BHCA blends (see Supporting Information). Among the three additives employed in this work, the SAXS data indicate that BHCA enhances the segregation strength most effectively followed by CTMA and then HHB. Therefore, BHCA blends form the highest domain spacing followed by CTMA and then HHB.

The strength of interaction of the additives with PEO chain segments and consequently their miscibility with PEO phase can be compared by comparing the DSC thermograms of neat F108 with that of various blends.⁹ The DSC thermograms obtained between -60 and 75 °C for neat F108 and its blend with the additives BHCA, HHB, and CTMA are shown in Figure 7. The thermograms for the blends were shifted vertically by adding constant values to heat flow. The values of the shifts are given in parentheses beside the thermograms. Neat F108 is characterized by a melting endotherm associated entirely with the melting of PEO crystallites because PPO does not crystallize and therefore shows no melting. As the additives are blended, they associate with the PEO segments, impede their crystallization, and cause a lowering of the PEO melting temperature. The general trend observed upon blending additives is that the melting endotherm peak becomes smaller and its peak position shifts systematically to lower temperatures, which indicates molecular scale interaction and of the additives with PEO chains. The behavior of the three additives can be better compared by comparing the melting enthalpies normalized by the weight of PEO in the blends and the melting temperatures represented by the endotherm peak positions. These comparisons are plotted in Figure 8 as a function of the blend compositions. BHCA caused maximum changes in these values from neat F108, indicating the strongest interaction with PEO which is consistent with the earlier mentioned observations of least FWHM of the primary scattering peaks and largest domain spacing for BHCA blends. The interaction of HHB with PEO is the weakest out of the three additives while CTMA ranges in between BHCA and HHB. It is clear from this data that while all the three additives showed favorable enthalpic interaction with PEO, carboxylic acid groups promote stronger interaction with PEO chains than phenol groups.

A smaller change in melting enthalpy for HHB blends also supports the finding from SAXS that hydrogen bond strength between HHB and PEO is less than the hydrogen bond strength between BHCA and PEO. Since PEO has a strong

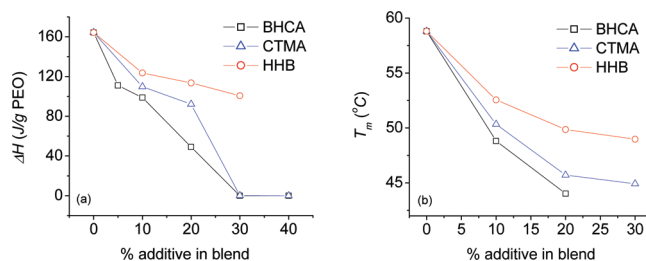


Figure 8. Analysis of endotherm peaks obtained for blends with varying BHCA, HHB, and CTMA compositions: (a) melting enthalpy normalized by the PEO concentration in the blends; (b) melting temperatures corresponding to the endotherms.

tendency to crystallize, weaker interaction energy of PEO with HHB allows more PEO segments to crystallize.

Conclusions and Outlook

We find that blending of small molecule additives that bear hydrogen-bonding sites for PEO at multiple locations can induce order in otherwise disordered Pluronic surfactants due to strong association with the PEO chains. Favorable hydrogen-bonding interaction between the additive molecules and PEO blocks causes selective incorporation of high loadings of the additives into the PEO phase. With increasing amount of additives in the blends OOT from cylindrical to spherical morphology occurred, and in the case of CTMA, this was followed by an order-to-disorder transition.

The availability of Pluronic surfactants with a wide range of relative volume fractions of PEO and PPO and the possibility of enriching them with a wide variety of readily available additives having various chemical attributes and molecular structures provide a rather general route to formation of BCP templates with phase selective functionalization with different morphologies and continuous range of domain spacings. Judicious choice of the additive allows formation of BCP templates selectively functionalized with different chemical groups. Moreover, variation of the core structure will enable the design of functional or structural materials. For example, we have extended this strategy to phase selective assembly of large aromatic molecules including molecular glasses for use as etch masks and inorganic cores including polyhedral silsesquioxane and nanoparticles to form highly loaded and well-ordered polymer nanocomposites (manuscript in preparation). While the assembly described here should be generally applicable to block copolymer/additive systems containing complementary hydrogen bond donors and acceptors, the realization of well-ordered materials that are templated entirely from commercially available BCP surfactants offer advantages to traditional BCPs in terms of availability, scalability, and cost.

It is observed that when sufficient amount of additives that are capable of interacting with PEO are added, in addition to the phase segregation to form ordered morphologies, the crystallization

of PEO is also suppressed. In addition, the blends studied were solidlike even at 80 °C whereas F108 is liquid at this temperature. Reduction in crystallinity of PEO while maintaining solidlike consistency is important for application of PEO and PEO-based block copolymers toward polymer electrolytes in rechargeable lithium ion batteries. For example, significant efforts have been made to reduce the crystallinity of PEO, thereby increasing its ionic conductivity by incorporation of salts and nanofillers.^{56–59} In addition, the need for high mechanical integrity has been addressed by employing PEO-containing BCPs in which the other block provides the necessary mechanical strength as well as constraints by which the ion conduction paths become well-defined.^{33,60,61} The present work hints at the design rules for additives in terms of their molecular architecture and chemical functionality which can be effective in altering the properties of PEO-based polymers.

Acknowledgment. This work was supported by the NSF Center for Hierarchical Manufacturing at the University of Massachusetts (CMMI-0531171).

Supporting Information Available: SAXS profiles in the range of 60–120 °C for neat F108 and its blend with BHCA at 10% and 20% loading. This material is available free of charge via the Internet at <http://pubs.acs.org>.

References and Notes

- Bates, F. S.; Fredrickson, G. H. *Phys. Today* **1999**, *52*, 32–38.
- Leibler, L. *Macromolecules* **1980**, *13*, 1602–1617.
- Bates, F. S.; Fredrickson, G. H. *Annu. Rev. Phys. Chem.* **1990**, *41*, 525–57.
- La, Y. H.; Park, S. M.; Meagley, R. P.; Leolukman, M.; Gopalan, P.; Nealey, P. F. *J. Vac. Sci. Technol., B* **2007**, *25*, 2508–2513.
- Park, S.; Lee, D. H.; Xu, J.; Kim, B.; Hong, S. W.; Jeong, U.; Xu, T.; Russell, T. P. *Science* **2009**, *323*, 1030–1033.
- Ruiz, R.; Kang, H. M.; Detcheverry, F. A.; Dobisz, E.; Kercher, D. S.; Albrecht, T. R.; de Pablo, J. J.; Nealey, P. F. *Science* **2008**, *321*, 936–939.
- Bitá, I.; Yang, J. K. W.; Jung, Y. S.; Ross, C. A.; Thomas, E. L.; Berggren, K. K. *Science* **2008**, *321*, 939–943.
- Pai, R. A.; Humayun, R.; Schulberg, M. T.; Sengupta, A.; Sun, J. N.; Watkins, J. J. *Science* **2004**, *303*, 507–510.
- Tirumala, V. R.; Pai, R. A.; Agarwal, S.; Testa, J. J.; Bhatnagar, G.; Romang, A. H.; Chandler, C.; Gorman, B. P.; Jones, R. L.; Lin, E. K.; Watkins, J. J. *Chem. Mater.* **2007**, *19*, 5868–5874.
- Nagarajan, S.; Li, M. Q.; Pai, R. A.; Bosworth, J. K.; Busch, P.; Smilgies, D. M.; Ober, C. K.; Russell, T. P.; Watkins, J. J. *Adv. Mater.* **2008**, *20*, 246–251.
- Hillmyer, M. A. Nanoporous materials from block copolymer precursors. In *Block Copolymers II*; Springer-Verlag: Berlin, 2005; Vol. 190, pp 137–181.
- Kang, M.; Moon, B. *Macromolecules* **2009**, *42*, 455–458.
- Luchnikov, V.; Kondyurin, A.; Formanek, P.; Lichte, H.; Stamm, M. *Nano Lett.* **2007**, *7*, 3628–3632.
- Misner, M. J.; Skaff, H.; Emrick, T.; Russell, T. P. *Adv. Mater.* **2003**, *15*, 221–224.
- Sohn, B. H.; Cohen, R. E. *Acta Polym.* **1996**, *47*, 340–343.
- Barber, R. P.; Gomez, R. D.; Herman, W. N.; Romero, D. B. *Org. Electron.* **2006**, *7*, 508–513.
- Barrau, S.; Heiser, T.; Richard, F.; Brochon, C.; Ngov, C.; van de Wetering, K.; Hadziioannou, G.; Anokhin, D. V.; Ivanov, D. A. *Macromolecules* **2008**, *41*, 2701–2710.
- Yang, C.; Lee, J. K.; Heeger, A. J.; Wudl, F. *J. Mater. Chem.* **2009**, *19*, 5416–5423.
- Fink, Y.; Urbas, A. M.; Bawendi, M. G.; Joannopoulos, J. D.; Thomas, E. L. In *Block Copolymers As Photonic Bandgap Materials*; Workshop on Electromagnetic Crystal Structures, Laguna Beach, CA, Jan 04–06, 1999; IEEE-Inst Electrical Electronics Engineers Inc.: Laguna Beach, CA, 1999; pp 1963–1969.
- Urbas, A.; Sharp, R.; Fink, Y.; Thomas, E. L.; Xenidou, M.; Fetters, L. J. *Adv. Mater.* **2000**, *12*, 812–814.
- Urbas, A.; Fink, Y.; Thomas, E. L. *Macromolecules* **1999**, *32*, 4748–4750.
- Kim, H. C.; Park, S. M.; Hinsberg, W. D. *Chem. Rev.* **2010**, *110*, 146–177.
- Mayes, A. M.; Delacruz, M. O. *J. Chem. Phys.* **1989**, *91*, 7228–7235.
- Matsen, M. W.; Thompson, R. B. *J. Chem. Phys.* **1999**, *111*, 7139–7146.
- Balazs, A. C.; Emrick, T.; Russell, T. P. *Science* **2006**, *314*, 1107–1110.
- Zhao, Y.; Hashimoto, T.; Douglas, J. F. *J. Chem. Phys.* **2009**, *130*, 1568–1582.
- van Zoelen, W.; ten Brinke, G. *Soft Matter* **2009**, *5*, 1568–1582.
- Bondzic, S.; de Wit, J.; Polushkin, E.; Schouten, A. J.; ten Brinke, G.; Ruokolainen, J.; Ikkala, O.; Dolbnya, I.; Bras, W. *Macromolecules* **2004**, *37*, 9517–9524.
- Tung, S. H.; Kalarickal, N. C.; Mays, J. W.; Xu, T. *Macromolecules* **2008**, *41*, 6453–6462.
- van Zoelen, W.; Asumaa, T.; Ruokolainen, J.; Ikkala, O.; ten Brinke, G. *Macromolecules* **2008**, *41*, 3199–3208.
- Ruokolainen, J.; Mäkinen, R.; Torkkeli, M.; Makela, T.; Serimaa, R.; ten Brinke, G.; Ikkala, O. *Science* **1998**, *280*, 557–560.
- Ruokolainen, J.; Saariaho, M.; Ikkala, O.; ten Brinke, G.; Thomas, E. L.; Torkkeli, M.; Serimaa, R. *Macromolecules* **1999**, *32*, 1152–1158.
- Singh, M.; Odusanya, O.; Wilmes, G. M.; Eitouni, H. B.; Gomez, E. D.; Patel, A. J.; Chen, V. L.; Park, M. J.; Fragouli, P.; Iatrou, H.; Hadjichristidis, N.; Cookson, D.; Balsara, N. P. *Macromolecules* **2007**, *40*, 4578–4585.
- Hawker, C. J.; Russell, T. P. *MRS Bull.* **2005**, *30*, 952–966.
- Sidorenko, A.; Tokarev, I.; Minko, S.; Stamm, M. *J. Am. Chem. Soc.* **2003**, *125*, 12211–12216.
- Kondyurin, A.; Bilek, M.; Janke, A.; Stamm, M.; Luchnikov, V. *Plasma Processes Polym.* **2008**, *5*, 155–160.
- Zschech, D.; Milenin, A. P.; Scholz, R.; Hillebrand, R.; Sun, Y.; Uhlmann, P.; Stamm, M.; Steinhart, M.; Goesele, U. *Macromolecules* **2007**, *40*, 7752–7754.
- Tokarev, I.; Krenek, R.; Burkov, Y.; Schmeisser, D.; Sidorenko, A.; Minko, S.; Stamm, M. *Macromolecules* **2005**, *38*, 507–516.
- Chen, J.; Frisbie, C. D.; Bates, F. S. *J. Phys. Chem. C* **2009**, *113*, 3903–3908.
- Epps, T. H.; Bailey, T. S.; Pham, H. D.; Bates, F. S. *Chem. Mater.* **2002**, *14*, 1706–1714.
- Epps, T. H.; Bailey, T. S.; Waletzko, R.; Bates, F. S. *Macromolecules* **2003**, *36*, 2873–2881.
- Hashimoto, T.; Tanaka, H.; Hasegawa, H. *Macromolecules* **1990**, *23*, 4378–4386.
- Tanaka, H.; Hasegawa, H.; Hashimoto, T. *Macromolecules* **1991**, *24*, 240–251.
- Lowenhaupt, B.; Steurer, A.; Hellmann, G. P.; Gallot, Y. *Macromolecules* **1994**, *27*, 908–916.
- Tirumala, V. R.; Daga, V.; Bosse, A. W.; Romang, A.; Ilavsky, J.; Lin, E. K.; Watkins, J. J. *Macromolecules* **2008**, *41*, 7978–7985.
- Tirumala, V. R.; Romang, A.; Agarwal, S.; Lin, E. K.; Watkins, J. J. *Adv. Mater.* **2008**, *20*, 1603–1608.
- Zhang, F. J.; Stuhn, B. *Colloid Polym. Sci.* **2006**, *284*, 823–833.
- Patrick, J.; Fairclough, A.; Yu, G. E.; Mai, S. M.; Crothers, M.; Mortensen, K.; Ryan, A. J.; Booth, C. *Phys. Chem. Chem. Phys.* **2000**, *2*, 1503–1507.
- Maurer, J. J.; Eustace, D. J.; Ratcliffe, C. T. *Macromolecules* **1987**, *20*, 196–202.
- The GaussAmp function of Origin software, $I = I_0 + Ae^{-(q-q^*)^2/2w^2}$ was used to fit the primary peak to obtain w . Here, I and I_0 represent the intensity along the curve and base intensity, respectively, and q^* represents the position of maximum I (i.e., peak position) and FWHM; w_1 was found as $w_1 = 2w(\ln 4)^{1/2}$.
- Lai, C. J.; Russel, W. B.; Register, R. A. *Macromolecules* **2002**, *35*, 4044–4049.
- The volume fraction vs interplanar spacing (ϕ_p, d) data for the three additives was fitted to the equation $d = A\phi_p^{-\beta}$ to find the three β values. A represents the hypothetical value of d for neat F108 because neat F108 is disordered. However, since the value of A should be the same in all the three cases, A was not fitted, but a value for it was determined such that the value of S —the sum of the sums of square of residuals for each data set—was minimized. Mathematically, S is denoted as $S = \sum_{\text{all additives}} \sum_{\text{each additive}} (Aw_p^{-\beta} - d)^2$. The inner summation represents the residuals for each additive's data set (i.e., the difference between calculated and experimental values of d) while the outer summation represents summation of residuals obtained for data sets of each additive.

- (53) Hashimoto, T.; Shibayama, M.; Kawai, H. *Macromolecules* **1983**, *16*, 1093–1101.
- (54) Mamodia, M.; Panday, A.; Gido, S. P.; Lesser, A. J. *Macromolecules* **2007**, *40*, 7320–7328.
- (55) Shibayama, M.; Hashimoto, T.; Kawai, H. *Macromolecules* **1983**, *16*, 16–28.
- (56) Kumar, B.; Rodrigues, S. J. *J. Electrochem. Soc.* **2001**, *148*, A1336–A1340.
- (57) Kumar, B.; Rodrigues, S. J.; Koka, S. *Electrochim. Acta* **2002**, *47*, 4125–4131.
- (58) Kumar, B.; Rodrigues, S. J.; Scanlon, L. G. *J. Electrochem. Soc.* **2001**, *148*, A1191–A1195.
- (59) Nookala, M.; Kumar, B.; Rodrigues, S. J. *Power Sources* **2002**, *111*, 165–172.
- (60) Gomez, E. D.; Panday, A.; Feng, E. H.; Chen, V.; Stone, G. M.; Minor, A. M.; Kisielowski, C.; Downing, K. H.; Borodin, O.; Smith, G. D.; Balsara, N. P. *Nano Lett.* **2009**, *9*, 1212–1216.
- (61) Panday, A.; Mullin, S.; Gomez, E. D.; Wanakule, N.; Chen, V. L.; Hexemer, A.; Pople, J.; Balsara, N. P. *Macromolecules* **2009**, *42*, 4632–4637.